THE JOURNAL OF PHYSICAL CHEMISTRY Letters

pubs.acs.org/JPCL

Letter

Interlayer Bonding in Two-Dimensional Materials: The Special Case of SnP_3 and GeP_3

Amine Slassi, Sai Manoj Gali, Anton Pershin,* Adam Gali, Jérôme Cornil, and David Beljonne*

Cite This: *J. Phys. Chem. Lett.* 2020, 11, 4503−4510

Read Online

ACCESS | Metrics & More | Article Recommendations | Supporting Information

ABSTRACT: Stacked two-dimensional (2D) heterostructures are evolving as the "next-generation" optoelectronic materials because of the possibility of designing atomically thin devices with outstanding characteristics. However, most of the existing 2D heterostructures are governed by weak van der Waals interlayer interactions that, as often is the case, exert limited impact on the resulting properties of heterostructures relative to their constituting components. In this work, we investigate the optoelectronic properties of a novel class of 2D MP_3 (M = Ge and Sn) materials featuring strong interlayer interactions, applying a robust theoretical framework combining density functional theory and many-body perturbation theory. We demonstrate that the remarkable intrinsic vertical strain (of ∼40% relative to the monolayers) promotes the exfoliation of these materials into bilayers and profoundly impacts their electronic structure, charge transport, and optical properties. Most strikingly, we observe that the strong interlayer hybridization indicates continuous optical absorption across the entire visible range that, together with high charge carrier mobility, makes these 2D MP_3 heterostructures attractive for photoconversion applications.

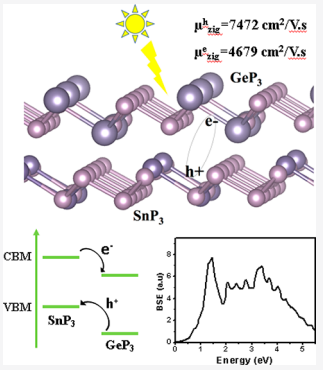

The world of electronics is dominated by silicon, in particular when it comes to field-effect transistors and photovoltaic devices.[1,2] Nowadays, a significant effort is dedicated to replace silicon by inexpensive analogues, both organic and/or inorganic in nature, which led to the emergence of new research directions, including, for example, flexible electronics and multifunctional devices.[3] While these alternative materials possess distinct advantages, it is still challenging to combine their exciting individual properties, for example, low weight and mechanical flexibility with high charge carrier mobility, in a functioning device. With the experimental discovery of graphene, and later of other members of the 2D family, such a combination is now within reach.[4−6]

Since the early days of 2D electronics, it was realized that 2D materials can benefit from the formation of vertical stacks with other monolayers. For instance, graphene shows its record carrier mobility when sandwiched between several layers of hexagonal boron nitride, likely protecting charge transport against scattering by Coulomb impurities at the dielectric interface.[7] The encapsulation of atomically thin black phosphorus between hexagonal boron nitride layers enabled the reduction of the interfacial scattering, thereby reaching high field-effect mobility of ∼1.350 $cm^2 V^{-1} s^{-1}$ at room temperature and ON/OFF ratios exceeding 10^5.[8] van der Waals (vdW) heterostructures are promising for photovoltaic applications because the resulting n−p junctions enable overcoming large exciton binding energies, permitting in turn the formation of free charge carriers.[9−11] Although efficient solar cells based on 2D heterostructures were realized,[12] the progress in this field is still limited, as the efficiency of the device is hampered by poor interlayer interactions, as evidenced by limited hybridization, and therefore reduced photoinduced charge generation. Alternatively, strong chemical interaction is achieved by coupling 2D materials in plane (known as lateral heterostructures).[13−15] In spite of its successful application, in-plane junctions feature limited contact interfaces and often suffer from harmful effects associated with lattice mismatch as well as of defects at grain boundaries.[16] Other possibilities to improve interlayer interactions include linking the layers by chemical tethers[17] or, as suggested here, taking advantage of natural bonded interactions between the monolayers.

Very recently, Woomer et al.[17] demonstrated that electrene (alternating layers of atoms and electrons) and graphene develop strong bonded interactions in vertical stacks, resulting in a transferred charge of 0.12 |e| per carbon atom (which is at least 2 orders of magnitude greater than in the existing van der Waals heterostructures).[10] Sreepal et al. showed that linked 2D sheets are also artificially accessible by chemical conversion of thin layered materials.[18] A strong interlayer interaction was also recently observed in sesqui-chalcogenides vertical stacks that are formed by a special interface bonding mechanism and characterized by strong electronic coupling at a relatively short

Received: March 10, 2020
Accepted: May 16, 2020
Published: May 16, 2020

interlayer distances (called van der Waals like distances[19]).[20] These findings are very intriguing and motivate us to explore the effects arising from bonded interactions in other conventional 2D materials. In this regard, the recently reported GeP_3 and SnP_3 bilayers are very attractive, because their crystal structures promise efficient interlayer coupling between the lone pairs of phosphorus and the metal atoms (see Figure 1a).

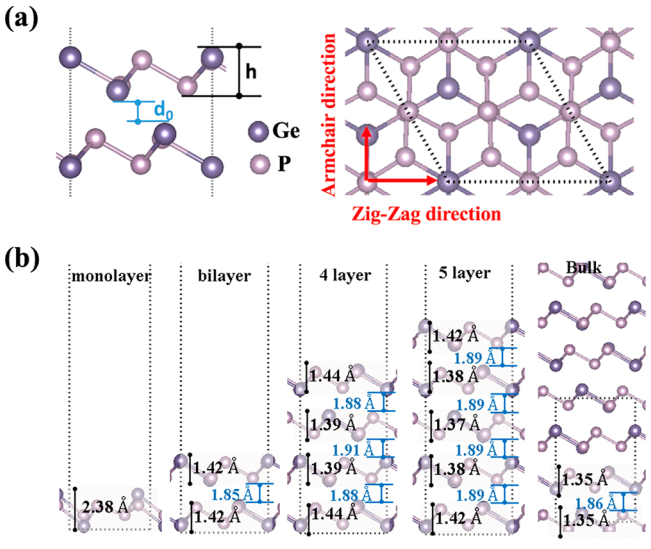

Figure 1. Structural representation of GeP_3 at equilibrium geometry with (a) top and side views of a unit cell of GeP_3 bilayer and (b) the geometry of GeP_3 as a function of the number of layers, illustrating the dimerization driven by bonded interactions and intrinsic strain at low dimensional level. The dashed black rhombus marks the unicell.

While former theoretical investigations on these materials indicate the presence of a moderate band gap combined with high charge carrier mobility at room temperature,[21−27] no investigation on the nature of the interactions and their impact on the optoelectronic properties has been reported to date, to the best our knowledge. Moreover, surprisingly, the calculated cleavage energies of GeP_3 monolayer from the bulk (~1.14 J·m^{-2})[21] and SnP_3 (~0.71 J·m^{-2} for monolayer and 0.45 J·m^{-2} for bilayer)[22] are close to those of graphene (~0.32 J·m^{-2}),[28] phosphorene (~0.36 J·m^{-2}), layered MoS_2 (0.29 J·m^{-2}),[29] Ga_2N (1.09 J·m^{-2}),[30] and GeS_2 (0.52 J·m^{-2}),[31] suggesting possible efficient exfoliation, but bringing into question strong bonding between monolayers. Furthermore, the phonon dispersion curves of GeP_3 and SnP_3 mono/bilayers show only real modes, demonstrating their stability.[21,26] These exciting but counterintuitive results require deeper investigations, especially at an advanced theoretical level.

In this work, we provide a systematic study of GeP_3 and SnP_3 bilayers and their heterostructures and assess their potential for photovoltaics based on a comprehensive theoretical investigation of their mechanical, electronic, optical, and transport properties. We identified that the small cleavage energy into bilayers rather than in monolayers arises from the pronounced inherent interlayer strain of magnitude as large as 1.3 eV/unit cell. Moreover, strong interlayer hybridization triggers unusual modifications of the electronic band structure, as evidenced by the appearance of a new band and additional valleys close to the conduction band minimum. Both effects in turn are found to be responsible for an increase in charge carrier mobility and the optical activation of dark states in a wide range of the visible spectrum. Finally, for the GeP_3/SnP_3 heterostructure, these interesting properties are accompanied by a remarkable charge transfer of 0.13 |e|/unit cell, which is among the largest values reported for vertical 2D stacks.

All DFT calculations were performed with the projector-augmented wave (PAW) basis set, as implemented in the VASP code.[32,33] The exchange and correlation effects are treated with the Perdew−Burke−Ernzerhof (PBE) functional,[34] incorporating the dispersion forces by the Grimme correction (PBE+D2) for structural relaxation.[35] PBE-GGA and HSE06 functionals, and quasi-particle energies $evGW_0$ theory are next employed in single-point calculations, applying a kinetic energy cutoff of 550 eV and using a Monkhorst−Pack mesh of 9 × 9 × 1 for the Brillouin zone (BZ) integration. Earlier studies showed that spin−orbit interaction has a minor impact on the band structure of these materials[21,22] and therefore was neglected in this work. In the converged $evGW_0$ calculations, the kinetic energy cutoff for the dielectric matrix was set to 140 eV and soft cutoff for Coulomb kernel was set to 320 eV, with the number of empty bands 8 times greater than that of occupied bands.

Before addressing the GeP_3/SnP_3 heterostructure, it is instructive to analyze the structural properties of the constitutive materials as well as of layered black phosphorus (P, taken as reference), as depicted in Figure 1 and S1 and summarized in Table S1. The lattice constants are calculated to be $a = b = 7.09$ Å and $c = 9.62$ Å for bulk GeP_3, and $a = b = 7.40$ Å and $c = 10.41$ Å, in good agreement with previous calculated values[21,26] and close to experimental data ($a = b = 7.05$ Å, $c = 9.93$ Å for bulk GeP_3,[36] and $a = b = 7.38$ Å, $c = 9.51$ Å for bulk SnP_3[37]). Upon decreasing the number of layers, MP_3 undergo a significant shrinkage of the lattice constant at 2D layers as shown in Figure S2. The lattice constant "a" of GeP_3-1L (1 layer) is slightly reduced relative to GeP_3-2L, indicating that GeP_3 undergoes a weak tensile lateral strain (0.15%) going from monolayer to bilayer. By contrast, the lattice constant of SnP_3-1L is significantly smaller than that of SnP_3-2L, resulting in a lateral tensile strain of 1.6%. The lattice constant of the GeP_3 monolayer is calculated to be 6.96 Å, while that of SnP_3 is 7.11 Å; therefore, this mismatch in the lattice constants between GeP_3 and SnP_3 monolayers induced a further lateral strain in the heterostructure: after full structural relaxation, the GeP_3 sheet undergoes a tensile strain of 1.8%, whereas the SnP_3 sheet is under a compressive strain of 0.2% (Figure S3 shows a marginal impact of lattice mismatch on the electronic structures).

Most importantly, in the GeP_3 and SnP_3 bilayers, the thickness of the constituting monolayers (h, in Figure 1) is reduced by ~40% compared to the individual (isolated) monolayers because of large structural relaxations (lateral) that manifest as *vertical* compressive strain. Furthermore, when going from the bulk phase to multilayered stacks, these materials exhibit a dimerization wherein the bilayer stacks are geometrically confined with no-negligible variations in the interlayer distance as well as in the intralayer thickness, as reported in Figures 1b and S1. This dimerization is a primary consequence of the modification in the interlayer interactions upon increasing the number of layers, which are inherently coupled to structural variations and the associated compressive/tensile strains. For example, the intralayer thickness of GeP_3 is 1.35 Å in its bulk phase compared to 2.38 Å when isolated (monolayer), with an interlayer thickness of 1.86 Å in the bulk (distance between topmost atom and bottommost

https://dx.doi.org/10.1021/acs.jpclett.0c00780
J. Phys. Chem. Lett. 2020, 11, 4503−4510

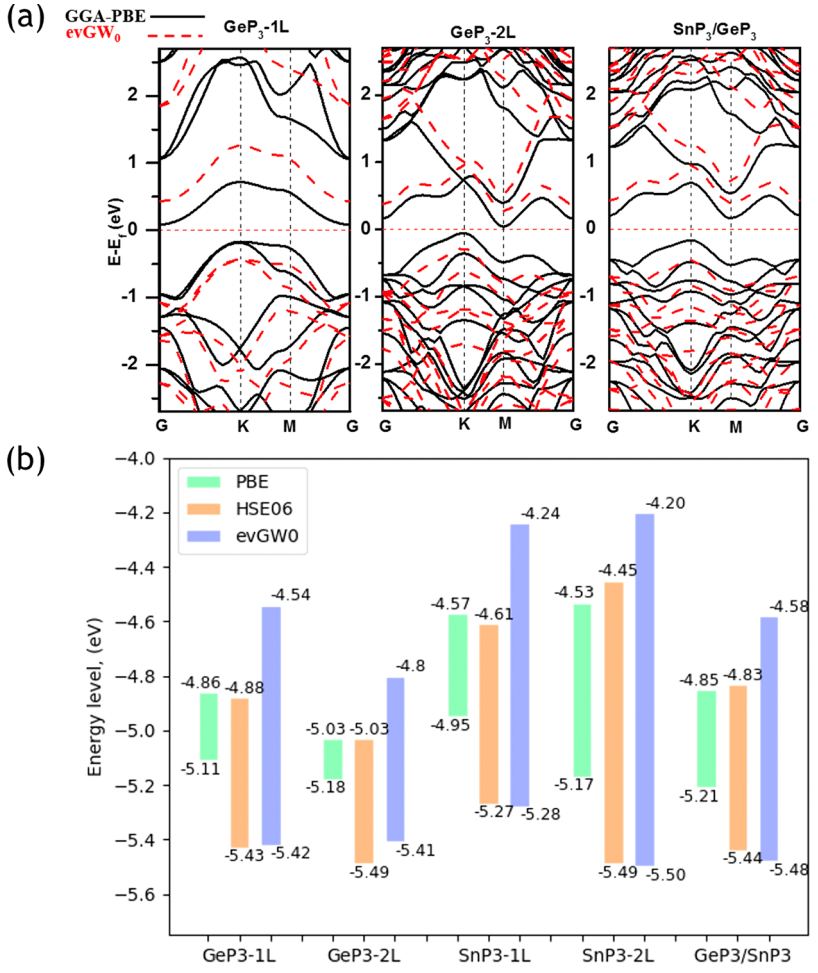

Figure 2. (a) Band structure of MP_3-1L (M = Ge or Sn) from PBE (solid) and evGW$_0$ (dashed lines) calculations. The Fermi level is taken as zero. (b) Theoretical band alignment of monolayers and bilayers of MP_3 (M = Ge or Sn) relative to the vacuum level. CBM and VBM calculated with the PBE and HSE06 functionals as well as at the evGW0 level; the quasiparticle band edges are positioned within the band gap-center approximation (see Figure S17).

atom). These distances tend to vary with increasing number of layers, as reported in Figure 1b for GeP_3. The structural reorganizations, caused by induced intrinsic strain, in turn lead to variations in the interlayer binding energies (E_B); E_B between two bilayer stacks for GeP_3 is calculated to be 1.94 eV/unit-cell in comparison to 4.65 eV between two unstrained monolayers in the bilayer conformation. This difference in the binding energies is due mostly to contribution arising from strain energy which in turn eases the exfoliation proceeding. The computed strain energies (the sum of strain energies for each monolayer) are 0.63 eV/unit-cell (GeP_3-2L), 1.35 eV/unit-cell (SnP_3-2L), and 1.14 eV/unit-cell (GeP_3/SnP_3), which are much greater than the nearly zero vertical strain in P-2L. Note that to track the variation in the stability of MP_3 from the bulk to monolayer, we calculated the variation in the cohesive energy as a function of the layer number, as shown in Figure S4. Accordingly, the small cohesive energy difference (0.06−0.25 eV) between MP_3 mono/bilayer and MP_3 bulk, which is in the same order of magnitude as that of phosphorene, verifies thermodynamically favorable exfoliation of stable 2D MP_3 phases from the bulk. The geometric changes associated with the inherent strain (see Figure S5) not only contribute to the stabilization of bilayers, therefore enabling easy exfoliation with a decrease in cleavage energy for bilayers as reported earlier,[22] but also point to strong interlayer interactions that are "bond-like" in contrast to conventional vdW interactions. The latter is confirmed by computing the intra- and interlayer bond-order parameters for the Ge−P bond in GeP_3-2L, yielding 0.7 and 0.35, respectively. These differ significantly from the corresponding values in archetypical vdW solids (0.95 for intralayer and 0.05 for interlayer P−P bond in P-2L). Furthermore, with the increase in the number of layers, the interlayer bond order decreases progressively, alongside the structural variations presented above. For instance, in a 4-layer system, the interlayer bond order is 0.21 between the central monolayers and 0.32 between the external ones.

To further shed light on the nature of interlayer interaction at interface layers, we analyzed the interatomic distances between Ge−P and Sn−P as in the percentage of the van der Waals radii of constituting atoms. The interatomic Ge−P and Sn−P bonds are found to be 61.9% and 61.7% relative to the sum of vdW radii of Ge and P (3.91 Å) and of Sn and P (3.97 Å), for GeP_3 and SnP_3, respectively. According to the bonding tetrahedron reported in ref 17, such values are closer to the weak covalent interactions (45−70%) than to so-called van der Waals like distances (70−95%).[19] These findings provide additional evidence for stronger interlayer coupling in MP_3 materials than upon forming 2D van der Waals stacks.

https://dx.doi.org/10.1021/acs.jpclett.0c00780
J. Phys. Chem. Lett. 2020, 11, 4503−4510

Table 1. Elastic Constant (C2D in N/m), Deformation Potential (E, in eV), and the Computed Electron and Hole Mobilities (μ, in $cm^2/(V\ s)$) of Monolayer and Bilayer of GeP_3 and SnP_3, along with That of the GeP_3−SnP_3 Heterostructure[a]

system	E_{Zig}	E_{Arm}	C_{zig}	C_{arm}	m_{zig}/m^*	m_{arm}/m^*	μ^{m}_{Zig}	τ^{m}_{Zig}(ps)	μ^{m}_{Arm}	τ^{m}_{Arm}(ps)	μ^{BTE}_{Zig}	τ^{BTE}_{Zig}(ps)	μ^{BTE}_{Arm}	τ^{BTE}_{Arm}(ps)
						GeP_3-1L								
e	3.81	3.81	22.01	22.04	1.28	1.27	13	0.009	53	0.038	21	0.016	22	0.016
h	1.91	1.43	22.01	22.04	0.75	0.58	152	0.065	136	0.045	51	0.022	120	0.040
						GeP_3-2L								
e	3.20	1.44	55.87	54.19	0.24	0.25	1343	0.184	5929	0.847	2260	0.31	7770	1.11
h	1.04	0.94	55.87	54.19	0.36	0.55	5652	1.162	2875	0.903	5347	1.10	4136	1.30
						SnP_3-1L								
e	2.59	2.75	39.50	39.58	1.23	0.67	55	0.038	165	0.063	130	0.092	214	0.082
h	0.90	0.97	39.50	39.58	1.13	0.87	541	0.349	788	0.391	326	0.211	366	0.182
						SnP_3-2L								
e	2.51	2.15	89.64	89.59	0.34	0.33	1745	0.339	2523	0.475	2228	0.433	3139	0.592
h	0.65	0.71	89.64	89.59	0.66	0.59	6907	2.604	7420	2.501	4141	1.562	3894	1.313
						SnP_3−GeP_3								
e	1.76	2.35	80.14	77.92	0.28	0.42	4679	0.748	1134	0.272	4500	0.72	1625	0.39
h	0.78	0.77	80.14	77.92	0.50	0.59	7472	2.134	5354	1.805	6265	1.79	5309	1.79

[a]Relaxation times (μ, in picoseconds) are also reported. Subscripts Arm and Zig correspond to the vales reported along the arm-chair direction and the zig-zag direction, respectively. $\mu_{Avg,\ model}$ corresponds to the mobility values computed for GeP_3 and SnP_3 monolayers using the elastic constant and deformation potential values of bilayers. μ^{m} corresponds to the mobilities obtained using effective mass; τ^{m} is computed using $\mu m^*/e$. μ^{BTE} corresponds to the mobility values obtained using the relaxation time from BoltzTrap code; τ^{BTE} is computed from BoltzTrap code. Mobility values for GeP_3−1L and SnP_3−1L using the stiffness constant of corresponding bilayers are also reported (model calculations).

Considering that this vertical strain also deforms the bond lengths (increase by ∼2%) and angles $\theta_{(P-P-P)}$ (increase by ∼10°), much greater modifications of the electronic structure are further expected, as compared to other 2D systems such as transition metal dichalcogenides (TMDs).[10]

The electronic band structure of MP_3, as predicted at the PBE and evGW$_0$ levels, is shown in Figure 2 (see also Figures S6−S10 and Table S2 for the band gaps). All mono- and bilayers of GeP_3 and SnP_3 are indirect bandgap semiconductors, while these materials start to exhibit metallic character upon increasing the number of layers beyond 3 layers (up to bulk[21,26]), as shown in Figure S11. Furthermore, the heterostructures formed by SnP_3-2L/GeP_3-1L or SnP_3-2L/GeP_3-2L also exhibit a metallic character as shown from the band structures in Figure S11. This semiconductor-to-metal transition can be explained by two main effects: (1) the strong dependence of interlayer interaction on the layer thickness and (2) the quantum confinement that may also plays an important role.[21,26] Interestingly, the bilayers built by removing the inherent strain, *i.e.*, by putting together two isolated sheets with the intralayer thickness pertaining to monolayers and interlayer distance of bilayers (to artificially remove the intrinsic strain in bilayers), are also semimetallic (as shown in Figures S12−S15). In the monolayers, the VBM is located at K-point, while the CBM is at G-point. The most important modification of the band structure caused by hybridization is the appearance of a new LUCO+1 band which is explicitly highlighted in Figure S16. Owning a large bandwidth, this new band effectively mixes with the LUCO, which in the case of GeP_3-2L and SnP_3/GeP_3 shifts the CBM from G-point to M-point and results in the formation of new valleys at M-point. Note that the effect is also present in SnP_3-2L but to a lesser extent that directly reflects the weaker interlayer bonding as evidenced by smaller cleavage energy for this material. We anticipate that the large dispersion around M should promote high electron mobility in the bilayers (see below). Moreover, similar to 2L-TMDs,[38] the degenerate (in monolayers) valence bands split by ∼0.36 eV into nondegenerate states around the VBM (at K-point) for all considered bilayers; such splitting was also reported to give rise to many interesting electronic, optical, and magnetic phenomena in TMDs.[39] Because of greater compressive strain and weaker mixing between LUCO and LUCO+1, the conduction band edge in the SnP_3 bilayer undergoes a significant upward shift in comparison to GeP_3 that, associated with a relatively greater downward shift of the valence band edge, leads to an increase in band gap in SnP_3 bilayers. As a result, from monolayer to bilayer, the (indirect) band gap decreases for GeP_3, while it increases for SnP_3.

Comparing the different levels of theory, the shape of the band structures is found to be similar, with the main difference being a simple rigid-band shift of the band edges opening the band gap when going from PBE to evGW$_0$, as shown in Figure 2a. The band gap calculated at the PBE level is underestimated by ∼50−100% as compared to HSE06, while evGW$_0$ calculations yield even greater values (see Table S2). In particular, at the evGW$_0$ level of theory, the GeP_3/SnP_3 heterostructure features a band gap of 0.90 eV that is intermediate to those of GeP_3 and SnP_3 bilayers (0.61 and 1.30 eV, respectively). Note that as shown in Figure S17 the convergence of the absolute quasiparticle band-edge energies by evGW$_0$ with increasing number of empty bands indicates that these materials obey the central band gap approximation (the correction shifts both CBM and VBM by equal amount but into the opposite directions relative to the values by KS-PBE) which is not the case for HSE06 that shows rather deeper levels of chemical potentials relative to PBE, in agreement with the HSE06 and evGW$_0$ results reported for MoS_2[40,41]. Irrespective of the level of theory, GeP_3-1L and SnP_3-1L form a staggered gap (type II) heterojunction that, together with a strong bonding, should induce a large ground-state (dark) charge transfer. In fact, a Bader charge analysis based on the HSE06 results demonstrates that ∼0.13 |e| per unit-cell is transferred from the SnP_3 layer to the GeP_3 layer, inducing a dipole moment of 0.28 D. In comparison, for the WSe_2/MoS_2 heterostructure, the transferred charge computed

https://dx.doi.org/10.1021/acs.jpclett.0c00780
J. Phys. Chem. Lett. 2020, 11, 4503−4510

at the same (HSE06) level of theory is only 0.015 lel per unit-cell and the dipole moment is 0.065 D.[10]

To access the implications of the changes in the electronic structure caused by the interlayer bonding on the charge transport properties, we calculated electron and hole band mobilities using the relaxation time approximation in conjunction with the semiclassical Boltzmann transport equation (BTE) (see the Supporting Information for details). Note that in the previous calculations of charge carrier mobility for GeP_3 and SnP_3,[21,26] the effective mass approximation was employed which in this case results in significant numerical discrepancies with BTE due to the complex shapes of the orbitals and the presence of degeneracies. The resulting mobility values for the monolayers and bilayers of GeP_3 and SnP_3, as well as the GeP_3/SnP_3 heterostructure, computed along the arm-chair and the zigzag directions, are reported in Table 1. In line with previous reports, the calculated mobility in both GeP_3 and SnP_3 bilayers are 2 orders of magnitude greater as compared to their corresponding monolayers; however, from our BTE calculation the values are even greater, reaching >7000 $cm^2/(V\ s)$ for GeP_3-2L. As demonstrated by the isoenergetic surface projection of VBM and CBM shown in Figure S18, this significant increase in mobility is due to the enhanced band dispersion in bilayers compared to their monolayer counterparts, which is a direct consequence of the interlayer bonding. In GeP_3-2L, the drastic increase of the electron mobility is mainly due to the decrease of the effective mass by a factor of 5 along both directions. In SnP_3-2L, this change is less pronounced; however, much greater values of the elastic constants still allow for efficient electron transport. As a results, the novel GeP_3/SnP_3 heterostructure takes advantage of the favorable properties from both materials and exhibits a fast transport channel along the zigzag direction, present in neither GeP_3-2L or SnP_3-2L. The latter results in the development of efficient ambipolar charge transport characteristics in the heterojunction, an essential parameter for photoactive/photoresponsive materials.

The computed mobility values represent a theoretical upper bound limit because so far only the acoustic phonon scattering was taken into account. In order to get a preliminary idea about scattering at point defects, which are inevitably generated in 2D materials, we analyzed the electronic structure and formation energies of Ge and P-vacancies in layered GeP_3 considering one respective defect in a 4 × 4 supercell. To this end, the computed band structures in Figure S19 suggest that neutral Ge and P defects tend to develop localized states outside the band gap and therefore should induce only limited impact on the resulting mobility. By contrast, in the bilayers, Ge_V and P_V develop shallow trap states close to conduction and valence bands, respectively, which might lower the mobility values. The relatively small formation energies of neutral defects predicted as a function of growing conditions (varying from P-rich to Ge-rich conditions as shown in Figure S20), suggest that both Ge_V and P_V defects are possible. A quantitative analysis of the influence of defects on charge carrier mobility would require additional efforts to calculate charge transition energy levels and include scattering and/or trapping in transport simulations, which we recognize would be useful but is beyond the scope of this Letter.

The most spectacular manifestation of the bonded interlayer interaction can be seen on the optical absorption spectrum (see Figures 3 and S21). Here, the two sharp peaks located at ∼2 and ∼4 eV in the monolayers significantly red-shift (to

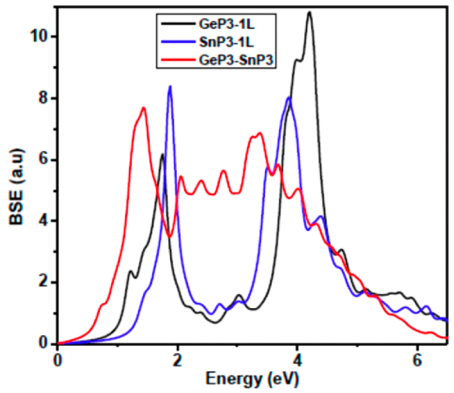

Figure 3. $evGW_0$/BSE spectra of GeP_3 monolayer, SnP_3 monolayer, and their heterostructure.

∼1.5 and ∼3.5 eV, respectively) in the heterostructure, while a continuous and strong optical absorption background develops across the whole intermediate wavelength region. Such effect of the strong interlayer interaction in developing a broad photoresponse was also experimentally and theoretically observed in layered platinum-based transition metal dichalcogenides[42,43]. It is clear that these changes should improve light harvesting in the visible and near-IR for photovoltaic applications. Note that the red shift and broadening of the spectra are also predicted in other MP_3-2L (see Figure S21) but not in P-2L. Decomposition of the absorption spectra into individual transitions (see Figure S22) reveals a rather cumulative increase of the intensity due to the large density of states, each bearing a modest contribution. The overall enhancement in optical absorption is again attributed to the interlayer bonding: all the new bright excitons feature the transitions to the new LUCO+1 band. The results shown in Figure S23 indicate that the artificial increase in the interlayer distance systematically reduces absorption intensity in the energy range from 2 to 4 eV (thereby recovering the spectra of constituting monolayers) and provides further evidence for the role of interlayer bonding.

Finally, to gain a detailed understanding of the origin of interlayer hybridization, we considered the case of an isolated Ge atom embedded into either P-1L or P-2L at the interface (Ge dopants substituting for P atoms), which can be viewed as an analogue of GeP_3 with a low density of adatoms. Interestingly, we find that the presence of a single isolated Ge atom develops into a manifold of localized states in the monolayer, with only one half-occupied state located inside the band gap (0.09 eV above the VBM). By contrast, in the bilayer, Ge atoms belonging to neighboring periodic unit cells couple over distances of at least 5 nm, resulting in the formation of a shallow band that extends along the arm-chair-direction (despite being rather localized along zigzag direction) (see Figure 4a). Such strong hybridization occurs because, in addition to the large interlayer interactions, there is close energy matching between the occupied localized state of the adatom-containing layer and the VBM of the other, pristine, P layer (see Figure 4b). This is confirmed by the Bader charge analysis that yields a charge transfer to the doped P-layer of ∼0.5 lel per adatom. The same effect is observed in GeP_3-2L; however, because of inversion symmetry, the charge transfer is bidirectional; that is, it simultaneously occurs from the top to the bottom layer and vice versa. This is best pictured by the charge density difference plots shown in Figure 4c, indicating a

https://dx.doi.org/10.1021/acs.jpclett.0c00780
J. Phys. Chem. Lett. 2020, 11, 4503−4510

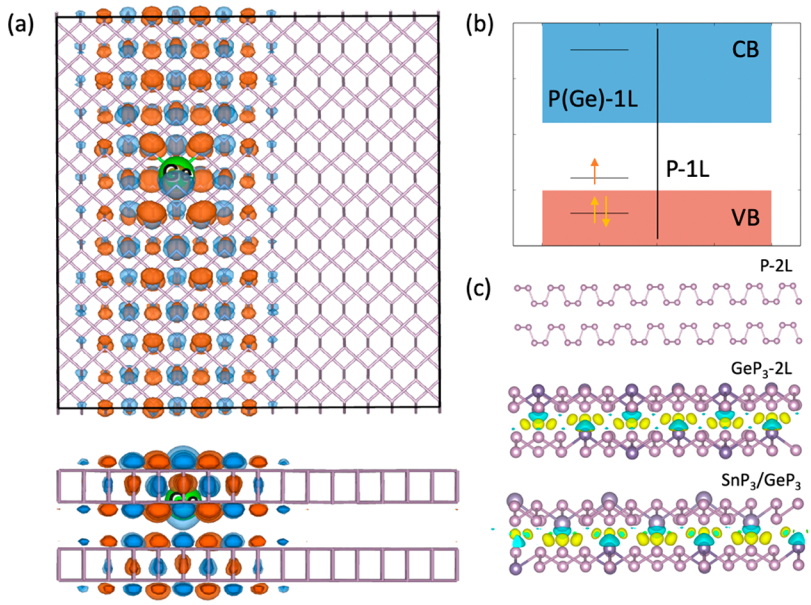

Figure 4. (a) Real space representation of one-electron wave function at G-point developed in P-2L due to the presence of a Ge atom. (b) Schematic representation of the electronic structures of P-1L containing one Ge atom and pristine P. (c) Difference between charge densities of the bilayer and the two constituting monolayers, computed for P-2L, GeP_3-2L, and SnP_3/GeP_3.

strong interfacial polarization, which originates from large and localized charge transfer from Ge-atom to the three nearest P-atoms in the surrounding layer. In turn, for the SnP_3/GeP_3 heterostructure, the type II alignment shifts the equilibrium toward the accumulation of electrons in the GeP_3 layer, resulting in the observable transferred charge of 0.13 |el| per unit cell. It is worth noting that the dispersion of the semilocalized states is largely reminiscent of the metallic states observed in the bulk. This enables us to conclude that the interlayer bonding occurs via the interaction between these defect states (each of them bearing one unpaired electron) and is mediated by structural relaxations.

In summary, by applying state-of-the-art many-body perturbation theory together with DFT calculations, we have systematically investigated the structural, electronic, optical, and transport properties of 2D MP_3 materials with specific emphasis on the impact of the bond-like interlayer interaction and the detailed mechanisms behind hybridization. It reveals that the individual sheets of these materials in their multilayer form undergo a remarkable intrinsic vertical strain (~40% relative to the monolayers) that plays a crucial role in the "easy" exfoliation of these materials into bilayers and in stabilizing their semiconducting properties. The bonding interaction between the layers manifests through the appearance of a new band close to CBM that together with intrinsic strain induces a profound rearrangement of the electronic structure of bilayers as compared to monolayers. In turn, these modifications in the electronic structure translate into a large improvement of charge-carrier mobility by 2 orders of magnitude and optical absorption cross-section covering the visible and infrared regions of the spectrum in the bilayers and heterostructure, making them suitable materials for photo-conversion applications. We hope that our theoretical work will prompt experimental exploration of these promising photo-active/photoreceptive materials.

■ ASSOCIATED CONTENT

Supporting Information

The Supporting Information is available free of charge at https://pubs.acs.org/doi/10.1021/acs.jpclett.0c00780.

Structural properties, electronic properties at equilibrium geometries, effect of intrinsic strain on the electronic structures, band structure edge convergences, transport properties, impact of point defects, and Bethe−Salpeter equation spectra (PDF)

■ AUTHOR INFORMATION

Corresponding Authors

Anton Pershin − *Laboratory for Chemistry of Novel Materials, Université de Mons, 7000 Mons, Belgium; Wigner Research Centre for Physics, H-1525 Budapest, Hungary;* Email: pershin.anton@wigner.hu

David Beljonne − *Laboratory for Chemistry of Novel Materials, Université de Mons, 7000 Mons, Belgium;* orcid.org/0000-0002-2989-3557; Email: David.BELJONNE@umons.ac.be

Authors

Amine Slassi − *Laboratory for Chemistry of Novel Materials, Université de Mons, 7000 Mons, Belgium;* orcid.org/0000-0001-5877-6045

Sai Manoj Gali − *Laboratory for Chemistry of Novel Materials, Université de Mons, 7000 Mons, Belgium;* orcid.org/0000-0002-0388-7888

Adam Gali − *Wigner Research Centre for Physics, H-1525 Budapest, Hungary; Department of Atomic Physics, Budapest University of Technology and Economics, H-1111 Budapest, Hungary;* orcid.org/0000-0002-3339-5470

Jérôme Cornil − *Laboratory for Chemistry of Novel Materials, Université de Mons, 7000 Mons, Belgium;* orcid.org/0000-0002-5479-4227

Complete contact information is available at: https://pubs.acs.org/10.1021/acs.jpclett.0c00780

https://dx.doi.org/10.1021/acs.jpclett.0c00780
J. Phys. Chem. Lett. 2020, 11, 4503−4510

Notes

The authors declare no competing financial interest.

■ ACKNOWLEDGMENTS

This work has been supported by the Belgian National Fund for Scientific Research (FRS-FNRS), Wallonie-Bruxelles international (WBI), and Region of Wallonie (RW) within the project of 2D Materials and FNRS-TOREADOR project. Computational resources were provided by the Consortium des Équipements de Calcul Intensif (CÉCI) funded by F.R.S.-FNRS under Grant 2.5020.11. A.P. acknowledges the financial support from the Marie Curie Fellowship (MILORD project, No. 748042). J.C. and D.B. are FNRS research directors. A.G. acknowledges the support from the National Office of Research, Development and Innovation in Hungary for Quantum Technology Program (Grant No. 2017-1.2.1-NKP-2017-00001) and National Excellence Program (Grant No. KKP129866). A.P. acknowledges the support from EU H2020 Quantum Technology Flagship project ASTERIQS (Grant No. 820394). We also thank Prof J. Coleman, from Dublin university, for sharing with us his latest data about liquid exfoliation of SnP_3 layers.

■ REFERENCES

(1) Tao, L.; Cinquanta, E.; Chiappe, D.; Grazianetti, C.; Fanciulli, M.; Dubey, M.; Molle, A.; Akinwande, D. Silicene. field-effect transistors operating at room temperature. *Nat. Nanotechnol.* **2015**, *10*, 227−231.

(2) Bullock, J.; Hettick, M.; Geissbühler, J.; Ong, A. J.; Allen, T.; Sutter-Fella, C. M.; Chen, T.; Ota, H.; Schaler, E. W.; De Wolf, S.; Ballif, C.; Cuevas, A.; Javey, A. Efficient silicon solar cells with dopant-free asymmetric heterocontacts. *Nat. Energy* **2016**, *1*, 15031.

(3) Huang, S.; Liu, Y.; Zhao, Y.; Ren, Z.; Guo, C. F. Flexible Electronics: Stretchable Electrodes and Their Future. *Adv. Funct. Mater.* **2019**, *29*, 1805924.

(4) Geng, D.; Yang, H. Y. Recent Advances in Growth of Novel 2D Materials: Beyond Graphene and Transition Metal Dichalcogenides. *Adv. Mater.* **2018**, *30*, 1800865.

(5) Manzeli, S.; Ovchinnikov, D.; Pasquier, D.; Yazyev, O. V.; Kis, A. 2D transition metal dichalcogenides. *Nat. Rev. Mater.* **2017**, *2*, 17033.

(6) Novoselov, K. S.; Mishchenko, A.; Carvalho, A.; Castro Neto, A. H. 2D materials and van der Waals heterostructures. *Science (Washington, DC, U. S.)* **2016**, *353*, aac9439.

(7) Quhe, R.; Zheng, J.; Luo, G.; Liu, Q.; Qin, R.; Zhou, J.; Yu, D.; Nagase, S.; Mei, W.-N.; Gao, Z.; Lu, J. Tunable and sizable band gap of single-layer graphene sandwiched between hexagonal boron nitride. *NPG Asia Mater.* **2012**, *4*, e6−e6.

(8) Chen, X.; Wu, Y.; Wu, Z.; Han, Y.; Xu, S.; Wang, L.; Ye, W.; Han, T.; He, Y.; Cai, Y.; Wang, N. High-quality sandwiched black phosphorus heterostructure and its quantum oscillations. *Nat. Commun.* **2015**, *6*, 7315.

(9) Furchi, M. M.; Pospischil, A.; Libisch, F.; Burgdörfer, J.; Mueller, T. Photovoltaic Effect in an Electrically Tunable van der Waals Heterojunction. *Nano Lett.* **2014**, *14*, 4785−4791.

(10) Slassi, A.; Cornil, J. Theoretical characterization of strain and interfacial electronic effects in donor-acceptor bilayers of 2D transition metal dichalcogenides. *2D Mater.* **2019**, *6*, No. 015025.

(11) Geim, A. K.; Van der Grigorieva, I. V. Waals heterostructures. *Nature* **2013**, *499*, 419−425.

(12) Ma, J.; Bai, H.; Zhao, W.; Yuan, Y.; Zhang, K. High efficiency graphene/MoS 2 /Si Schottky barrier solar cells using layer-controlled MoS 2 films. *Sol. Energy* **2018**, *160*, 76−84.

(13) Sun, Q.; Dai, Y.; Ma, Y.; Yin, N.; Wei, W.; Yu, L.; Huang, B. Design of lateral heterostructure from arsenene and antimonene. *2D Mater.* **2016**, *3*, No. 035017.

(14) Gong, Y.; Lin, J.; Wang, X.; Shi, G.; Lei, S.; Lin, Z.; Zou, X.; Ye, G.; Vajtai, R.; Yakobson, B. I.; Terrones, H.; Terrones, M.; Tay, B. K.; Lou, J.; Pantelides, S. T.; Liu, Z.; Zhou, W.; Ajayan, P. M. Vertical and in-plane heterostructures from WS2/MoS2 monolayers. *Nat. Mater.* **2014**, *13*, 1135−1142.

(15) Cheng, K.; Guo, Y.; Han, N.; Jiang, X.; Zhang, J.; Ahuja, R.; Su, Y.; Zhao, J. 2D lateral heterostructures of group-III monochalcogenide: Potential photovoltaic applications. *Appl. Phys. Lett.* **2018**, *112*, 143902.

(16) Zhou, W.; Zhang, Y.-Y.; Chen, J.; Li, D.; Zhou, J.; Liu, Z.; Chisholm, M. F.; Pantelides, S. T.; Loh, K. P. Dislocation-driven growth of two-dimensional lateral quantum-well superlattices. *Sci. Adv.* **2018**, *4*, No. eaap9096.

(17) Woomer, A. H.; Druffel, D. L.; Sundberg, J. D.; Pawlik, J. T.; Warren, S. C. Bonding in 2D Donor−Acceptor Heterostructures. *J. Am. Chem. Soc.* **2019**, *141*, 10300−10308.

(18) Sreepal, V.; Yagmurcukardes, M.; Vasu, K. S.; Kelly, D. J.; Taylor, S. F. R.; Kravets, V. G.; Kudrynskyi, Z.; Kovalyuk, Z. D.; Patanè, A.; Grigorenko, A. N.; Haigh, S. J.; Hardacre, C.; Eaves, L.; Sahin, H.; Geim, A. K.; Peeters, F. M.; Nair, R. R. Two-Dimensional Covalent Crystals by Chemical Conversion of Thin van der Waals Materials. *Nano Lett.* **2019**, *19*, 6475−6481.

(19) Alvarez, S. A cartography of the van der Waals territories. *Dalt. Trans.* **2013**, *42*, 8617.

(20) Cheng, Y.; Cojocaru-Mirédin, O.; Keutgen, J.; Yu, Y.; KüPers, M.; Schumacher, M.; Golub, P.; Raty, J.; Dronskowski, R.; Wuttig, M. Understanding the Structure and Properties of Sesqui-Chalcogenides (i.e., V 2 VI 3 or Pn 2 Ch 3 (Pn = Pnictogen, Ch = Chalcogen) Compounds) from a Bonding Perspective. *Adv. Mater.* **2019**, *31*, 1904316.

(21) Jing, Y.; Ma, Y.; Li, Y.; Heine, T. GeP 3: A Small Indirect Band Gap 2D Crystal with High Carrier Mobility and Strong Interlayer Quantum Confinement. *Nano Lett.* **2017**, *17*, 1833−1838.

(22) Ghosh, B.; Puri, S.; Agarwal, A.; Bhowmick, S. SnP 3: A Previously Unexplored Two-Dimensional Material. *J. Phys. Chem. C* **2018**, *122*, 18185−18191.

(23) Feng, L.-P.; Li, A.; Wang, P.-C.; Liu, Z.-T. Novel Two-Dimensional Semiconductor SnP 3 with High Carrier Mobility, Good Light Absorption, and Strong Interlayer Quantum Confinement. *J. Phys. Chem. C* **2018**, *122*, 24359−24367.

(24) Liu, C.-S.; Yang, X.-L.; Liu, J.; Ye, X.-J. Theoretical Prediction of Two-Dimensional SnP 3 as a Promising Anode Material for Na-Ion Batteries. *ACS Appl. Energy Mater.* **2018**, *1*, 3850−3859.

(25) Wang, Y.; Slassi, A.; Stoeckel, M.-A.; Bertolazzi, S.; Cornil, J.; Beljonne, D.; Samorì, P. Doping of Monolayer Transition-Metal Dichalcogenides via Physisorption of Aromatic Solvent Molecules. *J. Phys. Chem. Lett.* **2019**, *10*, 540−547.

(26) Sun, S.; Meng, F.; Wang, H.; Wang, H.; Ni, Y. Novel two-dimensional semiconductor SnP 3: high stability, tunable bandgaps and high carrier mobility explored using first-principles calculations. *J. Mater. Chem. A* **2018**, *6*, 11890−11897.

(27) Slassi, A.; Sorokin, P. B.; Pershin, A. Ohmic/Schottky barrier engineering in metal/SnP3 heterostructures. *J. Alloys Compd.* **2020**, *831*, 154800.

(28) Ziambaras, E.; Kleis, J.; Schröder, E.; Hyldgaard, P. Potassium intercalation in graphite: A van der Waals density-functional study. *Phys. Rev. B: Condens. Matter Mater. Phys.* **2007**, *76*, 155425.

(29) Björkman, T.; Gulans, A.; Krasheninnikov, A. V.; Nieminen, R. M.; van der Waals. Bonding in Layered Compounds from Advanced Density-Functional First-Principles Calculations. *Phys. Rev. Lett.* **2012**, *108*, 235502.

(30) Zhao, S.; Li, Z.; Yang, J. Obtaining Two-Dimensional Electron Gas in Free Space without Resorting to Electron Doping: An Electride Based Design. *J. Am. Chem. Soc.* **2014**, *136*, 13313−13318.

(31) Li, F.; Liu, X.; Wang, Y.; Li, Y. Germanium monosulfide monolayer: a novel two-dimensional semiconductor with a high carrier mobility. *J. Mater. Chem. C* **2016**, *4*, 2155−2159.

https://dx.doi.org/10.1021/acs.jpclett.0c00780
J. Phys. Chem. Lett. 2020, 11, 4503−4510

(32) Kresse, G.; Furthmüller, J. Efficient iterative schemes for ab initio total-energy calculations using a plane-wave basis set. *Phys. Rev. B: Condens. Matter Mater. Phys.* **1996**, *54*, 11169−11186.
(33) Kresse, G.; Marsman, M. *VASP the GUIDE*; 2012.
(34) Perdew, J. P.; Burke, K.; Ernzerhof, M. Generalized Gradient Approximation Made Simple. *Phys. Rev. Lett.* **1996**, *77*, 3865−3868.
(35) Grimme, S. Semiempirical GGA-type density functional constructed with a long-range dispersion correction. *J. Comput. Chem.* **2006**, *27*, 1787−1799.
(36) Donohue, P. C.; Young, H. S. Synthesis, structure, and superconductivity of new high pressure phases in the systems GeP and GeAs. *J. Solid State Chem.* **1970**, *1*, 143−149.
(37) Gullman, J.; Olofsson, O. The crystal structure of SnP3 and a note on the crystal structure of GeP3. *J. Solid State Chem.* **1972**, *5*, 441−445.
(38) Debbichi, L.; Eriksson, O.; Lebègue, S. Electronic structure of two-dimensional transition metal dichalcogenide bilayers from ab initio theory. *Phys. Rev. B: Condens. Matter Mater. Phys.* **2014**, *89*, 205311.
(39) Zhang, Y.; Li, H.; Wang, H.; Liu, R.; Zhang, S.-L.; Qiu, Z.-J. On Valence-Band Splitting in Layered MoS 2. *ACS Nano* **2015**, *9*, 8514−8519.
(40) Kang, J.; Tongay, S.; Zhou, J.; Li, J.; Wu, J. Band offsets and heterostructures of two-dimensional semiconductors. *Appl. Phys. Lett.* **2013**, *102*, No. 012111.
(41) Liang, Y.; Huang, S.; Soklaski, R.; Yang, L. Quasiparticle band-edge energy and band offsets of monolayer of molybdenum and tungsten chalcogenides. *Appl. Phys. Lett.* **2013**, *103*, No. 042106.
(42) Yuan, J.; Sun, T.; Hu, Z.; Yu, W.; Ma, W.; Zhang, K.; Sun, B.; Lau, S. P.; Bao, Q.; Lin, S.; Li, S. Wafer-Scale Fabrication of Two-Dimensional PtS 2 /PtSe 2 Heterojunctions for Efficient and Broad band Photodetection. *ACS Appl. Mater. Interfaces* **2018**, *10*, 40614−40622.
(43) Zhao, Y.; Qiao, J.; Yu, P.; Hu, Z.; Lin, Z.; Lau, S. P.; Liu, Z.; Ji, W.; Chai, Y. Extraordinarily Strong Interlayer Interaction in 2D Layered PtS 2. *Adv. Mater.* **2016**, *28*, 2399−2407.

https://dx.doi.org/10.1021/acs.jpclett.0c00780
J. Phys. Chem. Lett. 2020, 11, 4503−4510